Numerical analysis of 'On-Off' control thresholds and coolant flow rate for better performance of a Lithium-Ion battery thermal management system

R. Suresh Kumar[a,*], P.K. Rajesh[a], S. Neelakrishnan[a]

[a]*Department of Automobile Engineering, PSG College of Technology, Coimbatore, India*

(*Communicated by Madjid Eshaghi Gordji*)

Abstract

Electric vehicles will become an inevitable part of future transportation, because of the increasing concerns of global warming and climate change effects, caused by gasoline and diesel vehicles. Lithium-ion cells are the primary candidates for energy storage in electric vehicles. Lithium-ion cells are sensitive to operating temperatures. Operating them beyond the optimum temperatures, reduces their lifetime and can lead to thermal runaway, at extreme conditions. Hence, a thermal management system is required. In this work, a simple 'On-Off' control is used and the upper and lower thresholds are optimized, to reduce the energy consumption and the temperature difference between the cells. 3 coolant flow rates are selected and are analyzed for each upper and lower threshold. A MATLAB Simulink model and spreadsheet are used for analysis. The models are validated by experiments. It is found that a control strategy of $'32°C$ to $35°C'$, with a coolant flow rate of 0.67 kg s^{-1}, among the selected strategies, is better in reducing energy consumption and temperature difference. Running the cells at relatively higher temperatures, within the optimum range, helps in reducing energy consumption and temperature difference.

Keywords: Lithium-ion battery, Battery Thermal Management, On-Off control, Energy consumption, Temperature difference, Electric Vehicle.

*Corresponding author
   Email addresses: rsk.auto@psgtech.ac.in (R. Suresh Kumar), pkr.auto@psgtech.ac (P.K. Rajesh), snk.auto@psgtech.ac (S. Neelakrishnan)

1. Introduction

Lithium-ion cells are better candidates for electric vehicles as they combine the advantage of high power density and high energy density [15]. In addition, they have high nominal voltage and a low self-discharge rate [22]. They also have a long cycle life and no memory effect [33]. However, the lifetime and safety of these cells depend upon operating temperatures. The lifetime of these cells is an important factor in the ownership cost of electric vehicles. The battery pack accounts for a major portion of the entire vehicle's cost [20]. Repeated operation of the cells above $45°C$, degrades the electrodes and reduces the lifetime [12, 31, 17, 30]. The optimum operating temperature for lithium-ion cells is between $25°C$ to $40°C$ [18, 21]. This temperature range ensures better balance between lifetime and performance of the cells. Also, the initial temperature of the battery has to be within $40°C$, to ensure better charging efficiency at 1C rate [24]. In case of short circuits, a huge amount of heat is liberated in a short span of time. This may lead to thermal runaway. Also, overcharged cycling of lithium-ion batteries, can lead to earlier thermal runaway [19]. Although the battery management system (BMS) prevents over-charging and over-discharging, it can become faulty due to electromagnetic interference. To maintain the optimum temperature range of the cells and to ensure safety, a battery thermal management system (BTMS) is often required.

The BTMS can be either passive or active. Passive cooling takes place by natural convection, conduction or radiation. Whereas, active cooling spends energy to a fluid (air, water, etc.), to achieve desired cooling rate. In many cases, passive cooling is not sufficient to achieve desired performance, especially when the discharge rates are higher [23, 9]. Out of these, the most common and frequent methods are liquid cooling [14, 34, 28], air cooling [4], phase change material cooling [13, 11] or a combination of these [32].

Large temperature difference between the cells in a battery pack causes an unbalanced ageing of the battery. This can lead to an uneven mismatch of the internal resistances between cells. Generally, in a battery pack, all cells must have a similar charging and discharging rate. But, due to this mismatch, the overall life of the battery is reduced [30, 3]. Therefore, the temperature difference between the cells is also an important factor. The temperature difference between the cells should be maintained within $5°C$ [25]. In this work, active liquid cooling is considered, because it performs better in reducing the temperature difference between the cells [6].

Haoting Wang et al. [29] compared the energy consumptions of the BTMS, when operated normally and when operated with a simple 'On-Off' control. The results show that the 'On-Off' control can significantly reduce the energy consumptions of the system.

Although it has been already proposed that an 'On-Off' control can reduce energy consumption, there is a lack of investigation on the effects of upper and lower thresholds. Also, selecting a proper coolant flow rate is a trade-off between energy saving and temperature uniformity. This work will focus on how to select optimum upper and lower thresholds for the 'On-Off' control, along with the coolant flow rate.

1.1. Battery Sizing

The work starts with sizing the battery pack for Maruti Suzuki Alto car and designing a BTMS for it. The cell considered for this work is Samsung INR 18650-25R, which is a cylindrical lithium-ion cell. 18650 cylindrical cells are chosen, because they are easier to arrange and their lower volume and radius results in lower internal cell temperature difference and lower thermal inertia [27]. The parameters of the cell are given in table 1. The battery is sized according to the New European Driving cycle (NEDC). The resistive forces to the vehicle's motion are calculated and multiplied with instantaneous speed, to get the instantaneous power. The power is integrated over the operating

Table 1: Model and Experiment results for coolant pump operation time

Nominal Voltage	Nominal Capacity	Weight	Cathode	Anode	Cell Dimensions
3.2 V	2.5 Ah	45 grams	Nickel Cobalt Manganese Oxide (NMC)	Graphite-carbon	Height:64.85 $\pm$ 0.15 Diameter:18.33 $\pm$ 0.07

time, to get the energy required. The resistances considered are the drag resistance, rolling resistance and the inertial resistance. The values of drag co-efficient and frontal area are obtained from the work of Abdul Razaqque Anzari [2]. The respective formulas are listed below. The values of distance, speed and acceleration are taken from the NEDC.

$$Energy\ required = (Drag\ resistance + Rolling\ resistance + Inertial\ resistance) * Range \quad (1.1)$$

$$Drag\ resistance = 0.5 * Avf * Cd * vv2 * \rho \quad (1.2)$$

$$Rolling\ resistance = Cr * mv * g \quad (1.3)$$

$$Inertial\ resistance = mv * a \quad (1.4)$$

The density of air, ρ, is kept constant at 1.225 kg m-2. The rolling resistance co-efficient, Cr, is also considered as a constant, as the variations are negligible. The energy required for a range of 350 km is identified. It is divided by the driveline efficiency, which is assumed to be 80 percent. That energy is divided by the energy capacity of a single cylindrical cell, to get the total number of cells. The energy capacity of a cell is found by multiplying the nominal voltage (3.6 V) of the cell with the capacity (2.5Ah) and the available range of state of charge (80%). The total number of cells required is 4032. They are divided into 16 modules, with each module consisting of 252 cells, with 14 connected in series and 18 in parallel. The series-parallel arrangement is compact and is best suitable for the performance of BTMS [5]. The voltage output of each module is 50.4 V and nominal capacity is 45 Ah. 8 modules are connected in series, to make the entire battery voltage as 403.2 V and 2 such series strings are connected in parallel to make the battery capacity as 90 Ah. This is done, considering that, power-converters operating at 400 V, are available in the market.

2. Battery Assembly

Each module consists of 252 cylindrical cells, which are connected by 12P and 6P holders. The module assembly is shown in figures 1 and 2. One 12P and one 6P holder cells are connected in parallel. This makes 18 cells connected in parallel. 14 such combinations are placed in $7 * 2$ manner, such that these 14 combinations are connected in series. Aluminium plates containing copper tube, is placed in between these cells, in a serpentine manner. A thermal paste is used in between the cell and the aluminium plate, in order to maximize the area of contact. The cells are electrically connected by nickel strips. The nickel strips are spot welded to individual cell terminals. The assembled cells are placed in a battery fixture, during spot welding.
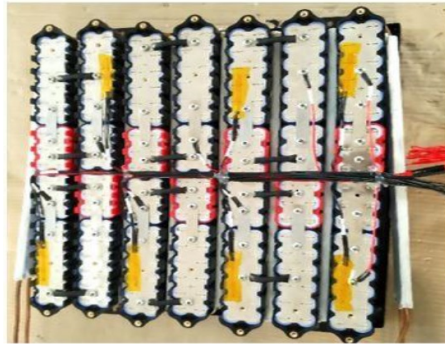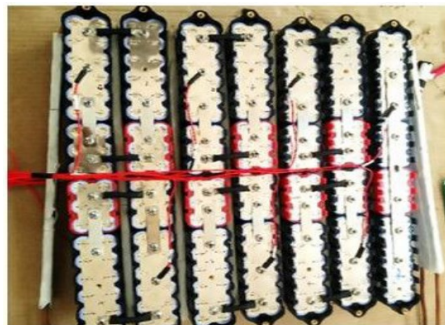
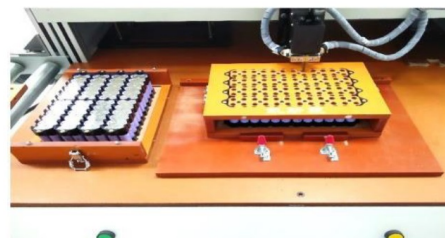Figure 1: Battery_(Top)

Figure 2: Battery_(Bottom)

Figure 3: Spot Welding of cell terminals

3. Simulink Model

3.1. Heat Generation

The heat generation in a lithium-ion cell can be divided into irreversible and reversible heat [1, 8, 7]. The irreversible heat is the product of the square of the current and the internal resistance of the cell. The internal resistance of the cell is taken from the works of Artur Kopczynski [10]. The reversible heat is due to the entropy of the reactions at the anode and the cathode. Reversible heat should also be considered, when the battery is cycled at lower C rates. [16]. They are found using the equations (3.3) and (3.4). The entropy of the cathode and anode is taken from the works of Viswanathan et al. [26].

$$qgen = qirr + qrev \qquad (3.1)$$

$$qirr = I2 * Rin \qquad (3.2)$$

$$qrev = IT(\partial E/\partial T) \qquad (3.3)$$

$$\Delta S = nF(\partial E/\partial T) \qquad (3.4)$$

In the above equations, Rin is the internal resistance, $(\partial E/\partial T)$ is the change of cell potential with respect to temperature, ΔS is the entropy change of the electrodes, n is the number of electrons during the experiment ($n = 1$ in this case) and F is the Faraday's constant. I is the current and it is positive during discharge and negative during charge.

3.2. Heat carried by coolant

The heat carried by the coolant, can be calculated using the relations (3.5),(3.6) and (3.7)

$$qout = U * Acl * (Tbatt - Tcl) \qquad (3.5)$$

$$U = 1/[(1/h) + (ri * \ln(ri/ro)/kcu) \qquad (3.6)$$

$$h = (Nu * kcl)/D \qquad (3.7)$$

Here, U is the overall heat transfer co-efficient. Acl is the inner curved surface area of the coolant channel. Tcl is the temperature of the coolant. The initial temperature of the coolant is assumed to be $25°C$, at the entry. The thermal resistance offered by the aluminium blocks are too low. Hence, they are neglected while identifying the total heat transfer co-efficient. kcu is the thermal conductivity of the copper tube.

The h is the convective heat transfer co-efficient and it is directly proportional to the Nusselt's number, Nu, and thermal conductivity of the coolant, kcl, and inversely proportional to the inner diameter of the coolant channel, D. The coolant is 50% ethylene glycol solution. ri and ro are the inner and outer radii of the coolant channel and kcu is the thermal conductivity of the copper tube.

3.3. Battery Temperature

The instantaneous battery temperature is identified by adding the initial temperature of the battery with the change in battery temperature caused by heat variations. The change in battery temperature is equal to the product of mass of the battery, specific heat capacity of the battery and the net heat generated or rejected.

$$Tbatt = Tini + \Delta Tbatt \tag{3.8}$$

$$Tbatt = Tini + mbatt * Cp, batt * (qgen - qout) \tag{3.9}$$

$qgen$ is always present, as the battery is discharged constantly and $qout$ is present when the coolant is passed and is equal to zero, when the coolant is not passed.

3.4. Energy Consumption

The energy consumption is the product of time, for which the coolant pump is operated, and the power required by the coolant pump. The coolant pump's operating time is identified by a Simulink model. The battery is discharged constantly at 0.2 C, 0.3 C, 0.4 C and the simulation is performed for a time period, corresponding to 80% depth of discharge of the battery. The simulation is performed for all the selected upper and lower thresholds and coolant flow rates. The initial temperature of the battery and the coolant temperature are kept at $25°C$.

The pump power can be identified by finding out the pressure losses in the system and kinetic energy required, for the respective flow rates. The pressure loss in metre, can be obtained using the Darcy-Weisbach equation,

$$hmajor = f * (L/D) * (vcl2/2g) \tag{3.10}$$

$$f = 64/Re \tag{3.11}$$

$$Re = \rho cl * vcl * D/\mu \tag{3.12}$$

f is the friction factor and is equal to 64 divided by Re, for laminar flows, where Re is the Reynolds number. ρcl is the density of the coolant, vcl is the velocity of the coolant, L is the length of the coolant channel, D is the inner diameter and g is the acceleration due to gravity.

This pressure loss, along with the kinetic energy in metre ($vcl2/2g$), represents the head required by the pump. The head required by the pump can be converted into the pump power using the relation (3.13).

$$P = \rho cl * g * Q * H/\eta \tag{3.13}$$

$$H = hmajor + vcl2/2g \tag{3.14}$$

where, Q is the volumetric flow rate of the coolant in m3 s-1 and H is the head required by the pump in m.

$$Energy\ Consumption = (Pump\ power) * (Operation\ time) \tag{3.15}$$

3.5. Temperature Difference

The temperature difference between the cells can be identified approximately, by performing the heat transfer and battery temperature relations, separately for the 16 modules. In other words, the temperature of the coolant is adjusted for successive battery modules. The temperature rise of the coolant through one module can be identified by equation (3.16).

$$qout = mcl * Cp, cl * (Tcl, out–Tcl, in) \tag{3.16}$$

$qout$ can be obtained from equation (3.5). Tcl, out and Tcl, in are the temperatures of the coolant exiting and entering the particular module. mcl is the mass flow rate and Cp, cl is the specific heat capacity of the coolant respectively. Tcl, out is found using the above equation and it is again used in equation (3.6) to find the heat rejected by the successive module. This process is repeated for all the modules, until the battery temperature of the first module reaches the lower limit of the selected control strategy. The battery temperature of the module, near to the coolant exit will be maximum, because of the increased coolant temperature. The temperature difference is identified by subtracting the last battery module temperature by the first battery module temperature.

3.6. Experimental Setup

The battery modules are connected and are maintained at a room temperature of $25°C$. A circulating pump is used, along with the coolant reservoir. The coolant pump is connected to another battery. The pump's volumetric discharge rate is approximately 0.22 kg s^{-1}. A thermistor is placed in the nearest cell to the coolant entry and also, in the farthest cell to the coolant entry. These thermistors are connected to a controller. The upper and lower thresholds of the control strategy are programmed in the controller and are set at $35°C$ to $28°C$ and $34°C$ to $27°C$. The controller also records the data of temperature versus time, from which the pumping time, for different lower thresholds can be assessed. The temperature difference can also be found from the data of the 2 thermistors. The battery is connected to a load of 0.3C, 0.4C and 0.5C. The coolant is passed into a condenser, after exiting from the battery pack.

4. Results and Discussion

4.1. Model Validation

The Simulink model and spreadsheet analysis are validated by comparing the results of the model with the experiment. The experiment is performed for 10 combinations of upper and lower thresholds, with a coolant flow rate of 0.22 kg s1. The coolant pump operation time and the temperature difference between the cells are recorded. The results of coolant pump operation time and temperature difference are provided in figures 5,6,7 and 8. Two experiments are done for the two different upper thresholds of $35°C$ and $34°C$.

The root mean square deviation for both the results are identified. The values of root mean square deviations are 15.17 and 0.05 for coolant pump operation time and temperature difference respectively. The deviation of 15.17 seconds for the coolant pump operation time is acceptable, as the energy requirements do not vary much for this value of deviation. Similarly, the deviation of $0.05°C$ for the temperature difference between the cells is also acceptable, as they might be caused due to the slight inaccuracy of the thermistor. The slight deviation can also be caused by the approximate modular level analysis and non-linearities of parameters like thermal conductivity and specific heat capacities. However, the model is still accurate for the purpose of ranking the strategies.

The coolant pump operation time and temperature difference are simulated for a number of different
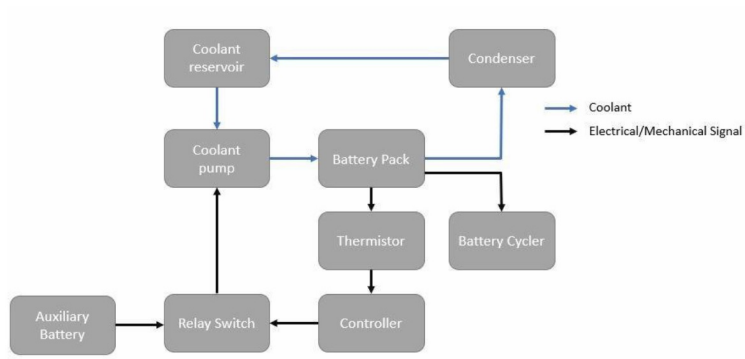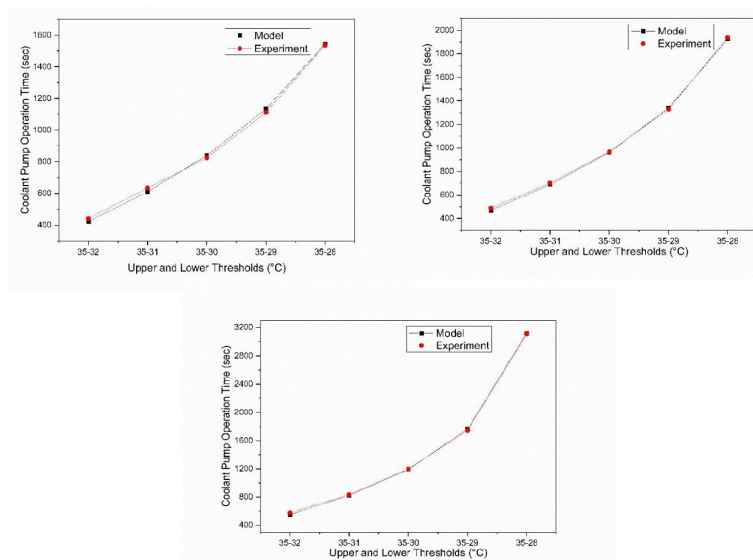
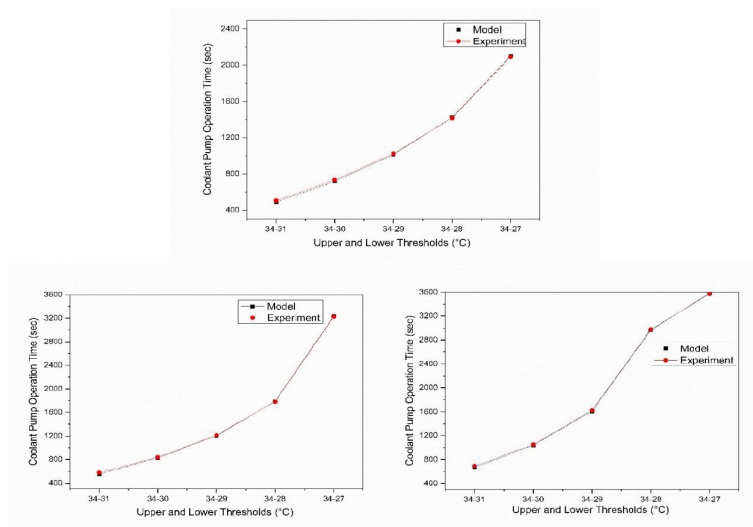Figure 4:

Figure 5: Coolant pump operation time

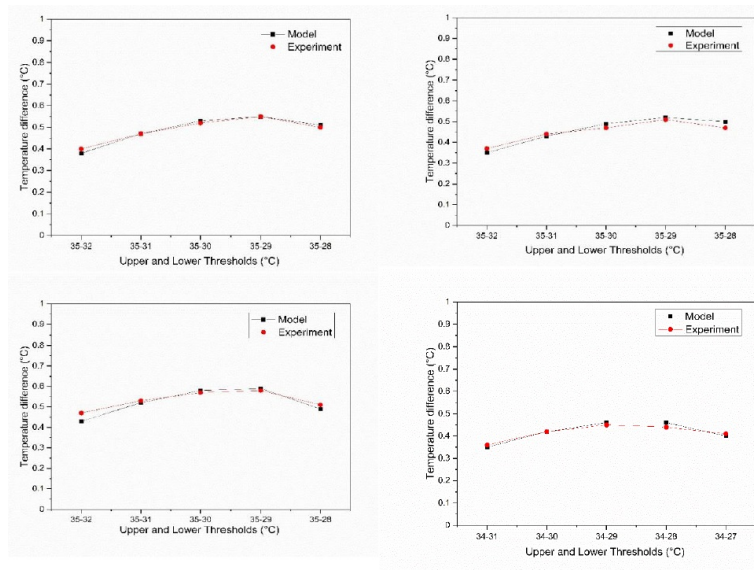Figure 6: Coolant pump operation time

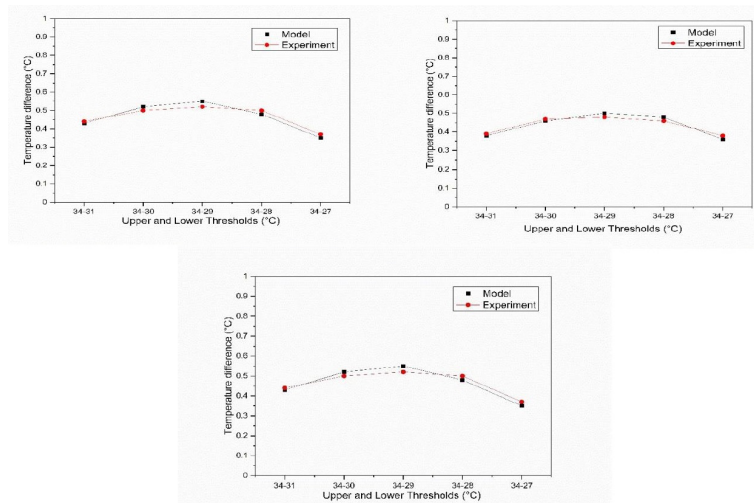Figure 7: Temperature difference
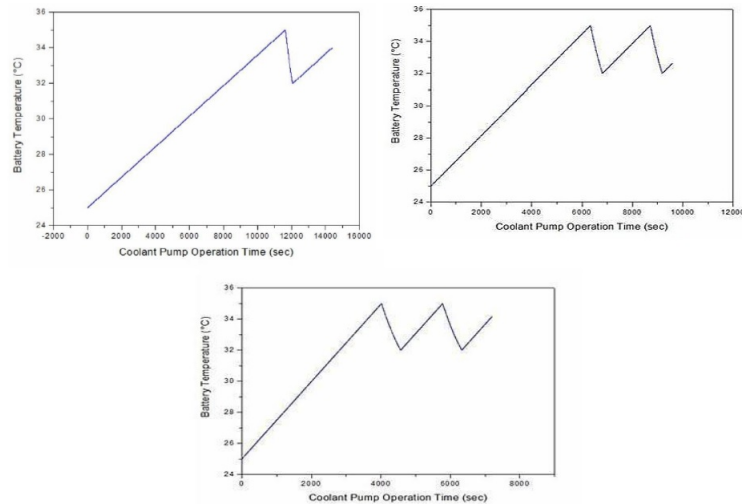

Figure 8: Temperature difference
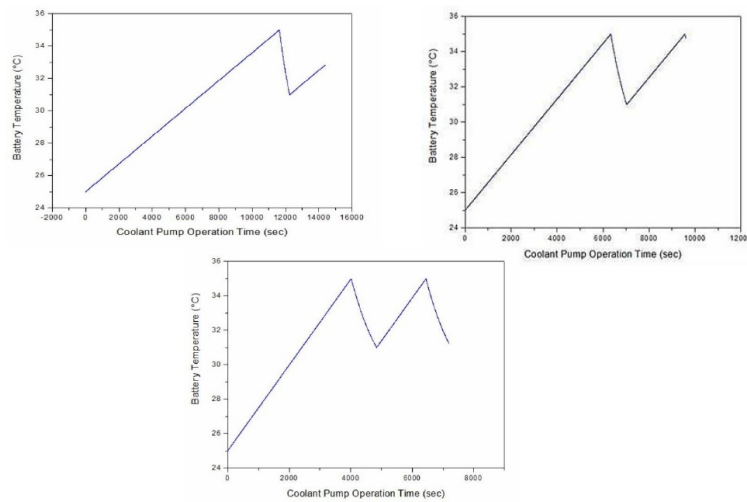
Figure 9: Battery Temperature

Figure 10: Battery Temperature

upper and lower thresholds, and for different coolant flow rates. An example of battery temperature oscillation between upper and lower thresholds of '$32°C to 35°C$', '$31°C to 35°C$', '$31°C to 34°C$' and '$30°C to 34°C$' are represented in figures 9,10,11 and 12.

In the above figures, the battery temperature rises sharply for higher discharge rates and vice versa. This is in accordance with the fact that, higher currents lead to higher heat generation and hence, higher temperature rise of the battery. When the coolant is passed, the battery temperature drops quickly for lower discharge rates and vice versa.

4.2. Scoring

'On-Off' control of different upper and lower thresholds, with 3 different coolant flow rates are simulated. The results of energy consumption and temperature difference between the cells are calculated, for each strategy. Based on the results, each strategy is awarded a score. Both the parameters (energy consumption, temperature difference between cells), are given equal weightages. The scoring is made in such a way that, higher energy consumption and higher temperature difference between cells, gets the highest score. Therefore, the strategy with the least score implies that, it
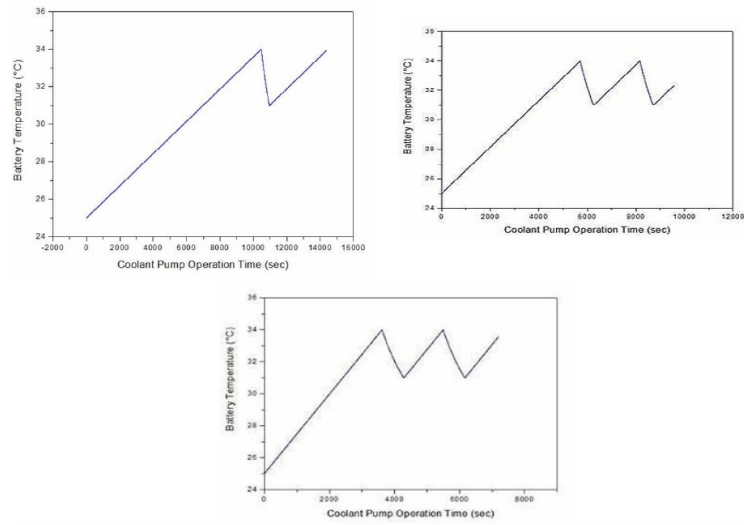
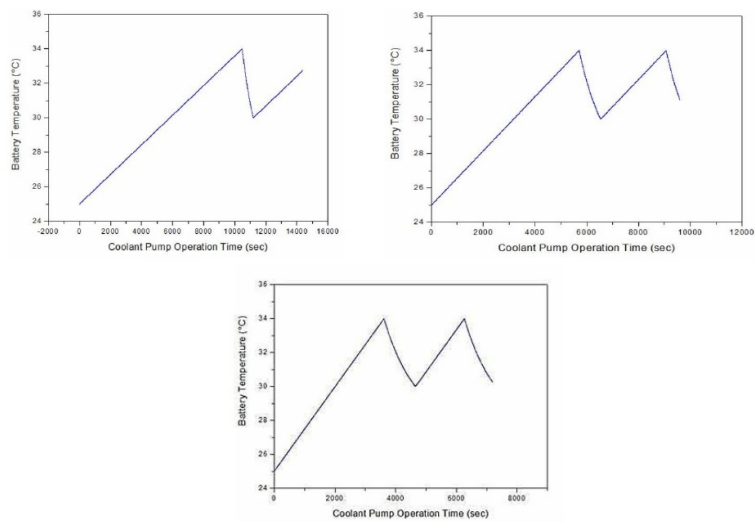Figure 11: Temperature difference

Figure 12: Battery Temperature

Table 2: Score chart for different strategies at 0.2C discharge

CONTROL STRATEGY	ENERGY CONSUMPTION (KWh)			TEMPERATURE DIFFERENCE (°C)			SCORE		
	0.68 kg s⁻¹	0.45 kg s⁻¹	0.22 kg s⁻¹	0.68 kg s⁻¹	0.45 kg s⁻¹	0.22 kg s⁻¹	0.68 kg s⁻¹	0.45 kg s⁻¹	0.22 kg s⁻¹
35 to 32 °C	0.62	0.28	0.07	0.12	0.18	0.35	9.2	12.2	29.8
35 to 31 °C	0.89	0.41	0.10	0.15	0.22	0.43	16.2	18.5	39.7
35 to 30 °C	1.23	0.56	0.14	0.17	0.25	0.49	22.8	24.0	47.3
35 to 29°C	1.66	0.76	0.19	0.18	0.26	0.52	29.4	27.6	51.5
35 to 28°C	2.26	1.03	0.26	0.17	0.25	0.5	35.8	29.9	50.0
35 to 27°C	3.25	1.48	0.38	0.14	0.21	0.42	44.7	30.8	41.9
34 to 31°C	0.71	0.33	0.08	0.12	0.18	0.35	10.4	12.7	29.9
34 to 30°C	1.05	0.48	0.12	0.14	0.21	0.42	17.0	18.2	38.7
34 to 29°C	1.48	0.67	0.17	0.16	0.23	0.46	24.8	23.0	44.1
34 to 28°C	2.08	0.95	0.24	0.16	0.23	0.46	32.3	26.5	45.0
34 to 27°C	3.08	1.40	0.36	0.13	0.2	0.4	41.3	28.6	39.3
33 to 30°C	1.69	0.77	0.20	0.12	0.17	0.34	22.7	17.1	30.1
33 to 29°C	1.28	0.58	0.15	0.14	0.2	0.4	19.9	18.3	36.7
33 to 28°C	1.88	0.86	0.22	0.14	0.21	0.42	27.4	22.9	39.9
33 to 27°C	2.87	1.31	0.33	0.13	0.19	0.38	38.7	26.3	36.6
32 to 29°C	2.08	0.95	0.24	0.11	0.17	0.33	26.4	19.4	29.5
32 to 28°C	2.33	1.06	0.27	0.13	0.19	0.37	31.9	23.1	34.6
32 to 27°C	2.64	1.20	0.31	0.12	0.18	0.35	34.6	23.7	32.7
31 to 28°C	2.73	1.25	0.32	0.11	0.16	0.31	34.6	21.9	28.1
31 to 27°C	4.03	1.84	0.47	0.11	0.16	0.32	50.9	29.3	31.2
30 to 27°C	4.06	1.85	0.47	0.1	0.14	0.28	50.0	27.1	26.4

consumes less energy and ensures better temperature uniformity than the other strategies. The results are provided in the tables2,3 and 4 for the discharge rates of 0.2 C, 0.3 C and 0.4 C respectively.

Some of the worst performing strategies are $30°C$ to $2°C$, with a flow rate of 0.68 kg s^{-1} and $34°C$ to $29°C$, with a flow rate of 0.22 kg s^{-1}. Lower operating temperatures reduces the heat rejection rate and hence, the system operation time increases. Also, a big difference between the upper and lower thresholds, result in increased operation time.

However, the results may vary, if the two parameters used for estimation (energy consumption, temperature difference between cells), are given different weightages. But it can be said that the results of this comparison, can be used to obtain a better balance between performance and lifetime of the battery.

Table 3: Score chart for different strategies at 0.3c discharge

CONTROL STRATEGY	ENERGY CONSUMPTION (KWh)			TEMPERATURE DIFFERENCE (°C)			SCORE		
	0.68 kg s⁻¹	0.45 kg s⁻¹	0.22 kg s⁻¹	0.68 kg s⁻¹	0.45 kg s⁻¹	0.22 kg s⁻¹	0.68 kg s⁻¹	0.45 kg s⁻¹	0.22 kg s⁻¹
35 to 32 °C	1.61	0.73	0.19	0.15	0.22	0.43	12.9	14.4	33.0
35 to 31 °C	2.30	1.05	0.27	0.18	0.27	0.52	20.7	21.8	43.2
35 to 30 °C	1.74	0.79	0.20	0.2	0.3	0.58	19.1	23.3	49.1
35 to 29°C	2.58	1.18	0.30	0.2	0.3	0.59	24.7	25.9	50.8
35 to 28°C	4.56	2.08	0.53	0.16	0.25	0.49	33.8	26.7	41.7
35 to 27°C	4.65	2.12	0.54	0.12	0.17	0.35	30.2	18.4	26.9
34 to 31°C	1.95	0.89	0.23	0.15	0.22	0.43	15.2	15.5	33.3
34 to 30°C	1.52	0.69	0.18	0.18	0.26	0.52	15.4	18.4	42.6
34 to 29°C	2.35	1.07	0.27	0.19	0.28	0.55	22.1	23.1	46.4
34 to 28°C	4.33	1.98	0.50	0.16	0.24	0.48	32.3	24.9	40.5
34 to 27°C	5.24	2.39	0.61	0.12	0.17	0.35	34.1	20.3	27.4
33 to 30°C	2.51	1.15	0.29	0.15	0.22	0.44	18.9	17.2	34.8
33 to 29°C	3.47	1.58	0.40	0.17	0.25	0.5	27.6	23.3	42.0
33 to 28°C	4.07	1.86	0.47	0.16	0.23	0.46	30.5	23.1	38.2
33 to 27°C	5.82	2.66	0.68	0.12	0.17	0.35	38.1	22.1	27.8
32 to 29°C	3.55	1.62	0.41	0.15	0.22	0.44	26.0	20.4	35.6
32 to 28°C	4.06	1.85	0.47	0.15	0.22	0.45	29.4	22.0	37.1
32 to 27°C	6.41	2.92	0.74	0.12	0.17	0.35	42.1	23.9	28.3
31 to 28°C	5.24	2.39	0.61	0.14	0.21	0.42	36.3	24.5	34.8
31 to 27°C	7.00	3.19	0.81	0.12	0.17	0.35	46.0	25.7	28.8
30 to 27°C	7.58	3.46	0.88	0.12	0.17	0.35	50.0	27.5	29.2

Table 4: Score chart for different strategies at 0.4C discharge

CONTROL STRATEGY	ENERGY CONSUMPTION (KWh)			TEMPERATURE DIFFERENCE (°C)			SCORE		
	0.68 kg s⁻¹	0.45 kg s⁻¹	0.22 kg s⁻¹	0.68 kg s⁻¹	0.45 kg s⁻¹	0.22 kg s⁻¹	0.68 kg s⁻¹	0.45 kg s⁻¹	0.22 kg s⁻¹
35 to 32 °C	1.37	0.63	0.16	0.13	0.2	0.38	5.9	15.1	31.4
35 to 31 °C	1.01	0.46	0.12	0.16	0.24	0.47	13.6	18.2	41.1
35 to 30 °C	1.41	0.64	0.16	0.18	0.27	0.53	18.9	23.0	48.1
35 to 29°C	1.95	0.89	0.23	0.19	0.28	0.55	24.3	26.0	50.9
35 to 28°C	2.81	1.28	0.33	0.18	0.26	0.51	29.8	26.8	47.2
35 to 27°C	4.71	2.15	0.55	0.13	0.18	0.37	39.0	24.7	33.3
34 to 31°C	1.62	0.74	0.19	0.14	0.2	0.38	16.1	15.9	31.7
34 to 30°C	1.93	0.88	0.22	0.16	0.23	0.46	20.7	20.4	40.8
34 to 29°C	1.76	0.80	0.20	0.17	0.25	0.5	20.5	22.0	45.1
34 to 28°C	2.62	1.19	0.30	0.17	0.24	0.48	27.2	23.9	43.7
34 to 27°C	4.73	2.16	0.55	0.12	0.18	0.36	38.0	24.7	32.2
33 to 30°C	1.97	0.90	0.23	0.13	0.19	0.38	17.7	16.1	32.0
33 to 29°C	2.85	1.30	0.33	0.15	0.22	0.44	26.8	22.5	39.4
33 to 28°C	2.39	1.09	0.28	0.16	0.23	0.45	24.3	22.0	40.1
33 to 27°C	4.50	2.05	0.52	0.12	0.17	0.35	36.3	22.8	30.9
32 to 29°C	2.54	1.16	0.29	0.13	0.19	0.37	22.1	18.1	31.4
32 to 28°C	3.78	1.72	0.44	0.14	0.21	0.41	32.9	24.7	36.9
32 to 27°C	4.24	1.93	0.49	0.12	0.17	0.34	34.2	21.9	29.6
31 to 28°C	3.61	1.65	0.42	0.12	0.18	0.36	29.4	20.8	31.2
31 to 27°C	4.70	2.15	0.55	0.11	0.17	0.32	36.7	23.5	27.8
30 to 27°C	6.56	2.99	0.76	0.1	0.16	0.3	50.0	29.0	27.2

5. Conclusion

The battery is sized for an approximate range of 350 km, for Maruti Suzuki Alto car, according to NEDC and the cells are assembled in a series-parallel configuration. 'On-Off' control of different upper and lower thresholds, with 3 different coolant flow rates are analyzed. A Simulink model is created to estimate the coolant pump operation time and the energy consumed by the system. The temperature difference between the cells within the pack is estimated using a spreadsheet analysis. The models are validated by comparing some of the results with the experimental results. Based on the model results, scores are given to each strategy. The strategy with the least score performs better. Upper and lower thresholds of $35°C$ and $32°C$, with a coolant flow rate of 0.68 kg s^{-1}, performs better than the other selected strategies. By interpreting the results of the strategies, the following can be concluded:

- Operating the cells at higher temperatures, within the optimum temperature limits, can greatly help in reducing the energy consumption of the system.

- Higher coolant flow rates can be used to keep the temperature difference between the cells as minimum as possible and higher upper and lower thresholds can be used to minimize the energy consumption.

- The difference between the upper and the lower threshold should be minimum and the thresholds should be closest to the highest temperature that is acceptable, to reduce the system operation time.

- Equal importance should be given to the design of radiator or condenser, to ensure minimum initial coolant temperature, which helps in reducing the energy consumption of the system.

Acknowledgments

References

[1] Y. Abdul-Quadir, T. Laurila, J. Karppinen, K. Jalkanen, K. Vuorilehto, L. Skogström and M. Paulasto-Kröckel, *Heat generation in high power prismatic Li-ion battery cell with $LiMnNiCoO_2$ cathode material*, Int. J. Energy Res. 38(11) (2014) 1424–1437.

[2] A. Abdul Razzaque and R. Prashant Kumar, *CFD analysis of aerodynamic design of maruti Alto car*, Int. J. Mechanical Eng. Tech. 8(3) (2017) 388–399.

[3] Z. An, L. Jia, Y. Ding, C. Dang and X. Li, *A review on lithium-ion power battery thermal management technologies and thermal safety*, J. Therm. Sci. 26(5) (2017) 391–412.

[4] K. Chen, Y. Chen, Y. She, M. Song, S. Wang and L. Chen, *Construction of effective symmetrical air-cooled system for battery thermal management*, Appl. Therm. Eng. 166 (2020) 114679.

[5] Y. Deng, C. Feng, J. E, H. Zhu, J. Chen, M. Wen and H. Yin, *Effects of different coolants and cooling strategies on the cooling performance of the power lithium ion battery system: A review*, Appl. Therm. Eng. 142 (2018) 10–29.

[6] H.S. Hamut, I. Dincer, G.F. Naterer, *Performance assessment of thermal management systems for electric and hybrid electric vehicles*, Int. J. Energy Res. 37(1) (2013) 1–12.

[7] J. Kang, G. Rizzoni, *Study of relationship between temperature and thermal energy, operating conditions as well as environmental factors in large-scale lithium-ion batteries*, Int. J. Energy Res. 38(15) (2014) 1994–2002.

[8] G. Karimi and X. Li, *Thermal management of lithium-ion batteries for electric vehicles*, Int. J. Energy Res. 37(1) (2012) 13–24.

[9] S.A. Khateeb, M.M. Farid, J.R. Selman and S. Al-Hallaj, *Design and simulation of a lithium-ion battery with a phase change material thermal management system for an electric scooter*, J. Power Sources 128(2) (2004) 292–307.

[10] A. Kopczyński, Z. Liu, P. Krawczyk, *Parametric analysis of Li-ion battery based on laboratory tests*, E3S Web of Conf. 44 (2018) 00074.

[11] A. Lazrak, J.-F. Fourmigué and J.-F. Robin, *An innovative practical battery thermal management system based on phase change materials: Numerical and experimental investigations*, Appl. Therm. Eng. 128 (2018) 20–32.

[12] F. Leng, C. Tan and M. Pecht, *Effect of temperature on the aging rate of Li Ion battery operating above room temperature*, Sci Rep. 5 (2015) 12967.

[13] Y. Li, Y. Du, T. Xu, H. Wu, X. Zhou, Z. Ling and Z. Zhang, *Optimization of thermal management system for Li-ion batteries using phase change material*, Appl. Therm. Eng. 131 (2018) 766–778.

[14] K. Li, J. Yan, H. Chen and Q. Wang, *Water cooling based strategy for lithium ion battery pack dynamic cycling for thermal management system*, Appl. Therm. Eng. 132 (2018) 575–585.

[15] Z. Ling, F. Wang, X. Fang, X. Gao and Z. Zhang, *A hybrid thermal management system for lithiumion batteries combining phase change materials with forced-air cooling*, Appl. Energy 148 (2015) 403–409.

[16] Z. Lu, X.L. Yu, L.C. Wei, F. Cao, L.Y. Zhang, X.Z. Meng and L.W. Jin, *A comprehensive experimental study on temperature-dependent performance of lithium-ion battery*, Appl. Therm. Eng. 158 (2019) 113800.

[17] M. Malik, I. Dincer and M.A. Rosen, *Review on use of phase change materials in battery thermal management for electric and hybrid electric vehicles*, Int. J. Energy Res. 40(8) (2016) 1011–1031.

[18] M. Malik, I. Dincer, M.A. Rosen, M. Mathew and M. Fowler, *Thermal and electrical performance evaluations of series connected Li-ion batteries in a pack with liquid cooling*, Appl. Therm. Eng. 129 (2018) 472–481.

[19] N. Mao, Z.-R. Wang, Y.-H. Chung and C.-M. Shu, *Overcharge cycling effect on the thermal behavior, structure, and material of lithium-ion batteries*, Appl. Therm. Eng. 163 (2019) 114147.

[20] N. Omar, D. Widanage, M. Abdel Monem Y. Firouz, O. Hegazy, P. Van den Bossche, T. Coosemans and J. Van Mierlo, O*ptimization of an advanced battery model parameter minimization tool and development of a novel electrical model for lithium-ion batteries*, Int. Trans. Electr. Energ. Syst. 24(12) (2013) 1747–1767.

[21] A.A. Pesaran, *Battery thermal models for hybrid vehicle simulations*, J. Power Sources 10(2) (2002) 377–382.

[22] A. Ritchie and W. Howard, *Recent developments and likely advances in lithium-ion batteries*, J. Power Sources 162(2) (2006) 809–812.

[23] R. Sabbah, R. Kizilel, J.R. Selman and S. Al-Hallaj, *Active (air-cooled) vs. passive (phase change material) thermal management of high power lithium-ion packs: limitation of temperature rise and uniformity of temperature distribution*, J. Power Sources 182(2) (2008) 630–638.

[24] M. Tan, Y. Gan, J. Liang, L. He, Y. Li, S. Song and Y. Shi, *Effect of initial temperature on electrochemical and thermal characteristics of a lithium-ion battery during charging process*, Appl. Therm. Eng. 177 (2020) 115500.

[25] N. Terada, *Development of lithium batteries for energy storage and EV applications*, J. Power Sources 100(1-2) (2001) 80–92.

[26] V.V. Viswanathan, D. Choi, D. Wang, W. Xu, S. Towne, R.E. Williford, J.-G. Zhang, J. Liu and Z. Yang, *Effect of entropy change of lithium intercalation in cathodes and anodes on Li-ion battery thermal management*, J. Power Sources 195(11) (2010) 3720–3729.

[27] S. Wang, K. Li, Y. Tian, J. Wang, Y. Wu and S. Ji, *An experimental and numerical examination on the thermal inertia of a cylindrical lithium-ion power battery*, Appl. Therm. Eng. 154 (2019) 676–685.

[28] H. Wang, T. Tao, J. Xu, X. Mei, X. Liu and P. Gou, *Cooling capacity of a novel modular liquid-cooled battery thermal management system for cylindrical lithium ion batteries*, Appl. Therm. Eng. 178 (2020) 115591.

[29] H. Wang, W. Xu, L. Ma, *Actively controlled thermal management of prismatic lithium-ion cells under elevated temperatures*, Int. J. Heat and Mass Transf. 102 (2016) 315–322.

[30] N. Yang, X. Zhang, G. Li and D. Hua, *Assessment of the forced air-cooling performance for cylindrical lithium-ion battery packs: a comparative analysis between aligned and staggered cell arrangements*, Appl. Therm. Eng. 80 (2015) 55–65.

[31] N. Yang, X. Zhang, B. Shang, B.B. Shang and S. Li, *Unbalanced discharging and aging due to temperature differences among the cells in a lithium-ion battery pack with parallel combination*, J. Power Sources 306 (2016) 733–741.

[32] W. Yang, F. Zhou, H. Zhou, Q. Wang and J. Kong, *Thermal performance of cylindrical lithium-ion battery thermal management system integrated with mini-channel liquid cooling and air cooling*, Appl. Therm. Eng. 175 (2020) 115331.

[33] Y. Ye, L.H. Saw, Y. Shi and A.A. Tay, *Numerical analyses on optimizing a heat pipe thermal management system for lithium-ion batteries during fast charging*, Appl. Therm. Eng. 86 (2015) 281–291.

[34] H. Zhang, C. Li, R. Zhang, Y. Lin and H. Fang, *Thermal analysis of a 6s4p Lithium-ion battery pack cooled by cold plates based on a multi-domain modeling framework*, Appl. Therm. Eng. 173 (2020) 115216.